Generating signals at converging liquid fronts to create line-format readouts of soluble assay products in three-dimensional paper-based devices

Ibrahim Abdullah[†], Daniel J. Wilson[†], Andrea C. Mora, Rayleigh W. Parker, and Charles R. Mace*

Department of Chemistry, Tufts University, Medford, MA 02155

[†] Authors contributed equally.

^{*}Corresponding author email: charles.mace@tufts.edu

Abstract

The correct interpretation of the result from a point-of-care device is crucial for an accurate and rapid diagnosis to guide subsequent treatment. Lateral flow tests (LFTs) use a wellestablished format that was designed to simplify the user experience. However, the LFT device architecture is inherently limited to detecting analytes that can be captured by molecular recognition. Microfluidic paper-based analytical devices (uPADs), like LFTs, have the potential to be used in diagnostic applications at the point of care. However, µPADs have not gained significant traction outside of academic laboratories, in part, because they have often demonstrated a lack of homogeneous shape or color in signal outputs, which consequently can lead to inaccurate interpretation of results by users. Here, we demonstrate a new class of µPADs that form colorimetric signals at the interfaces of converging liquid fronts (i.e., lines) to control where colorimetric signals are formed without relying on capture techniques. We demonstrate our approach by developing assays for three classes of analytes—an ion, an enzyme, and a small molecule—to measure using iron (III), acetylcholinesterase, and lactate, respectively. Additionally, we show these devices have the potential to support multiplexed assays by generating multiple lines in a common readout zone. These results highlight the ability of this new paper-based device architecture to aid the interpretation of assays that create soluble products by using flow to constrain those colorimetric products in a familiar, line-format output.

Introduction

Lateral flow test (LFT) strips have achieved widespread success in performing diagnostic tests at the point of care (POC) because their common architecture supports the development of a variety of immunoassay formats, utilizes scalable manufacturing processes to facilitate production and dissemination, and enables the interpretation of assay results by visual inspection. Nonetheless, the lateral flow device architecture largely limits testing to analytes that can be captured by immobilized molecular recognition agents (e.g., antibodies¹ or nucleic acids² and testing is predominantly qualitative (i.e., presence or absence of a test line), both of which inherently restrict how broadly LFTs can be applied as a platform for POC measurements.^{3,4} As an alternative to LFTs, paper-based microfluidic devices or microfluidic paper analytical devices (µPAD) have drawn recent appeal due to their potential to support a broader test menu than LFTs (e.g., cell counts, nucleic acid amplification, immunoassays),^{5–10} compatibility with a wide range of assay readout methods (e.g., colorimetric, fluorescent, electrochemical, chemiluminescent),¹¹

-15 ability to support device complexity (e.g., evaporative concentration, origami or "pop-up", fluid control valves)^{5,16,17,18} and utilize creative options for generating a user interface (e.g., wicking distance, timed readout, zones filled, and text appearance).^{19–23}

The first paper-based microfluidic device, and similarly many subsequent prototypes, demonstrated the detection of analytes (e.g., glucose and albumin) using chemistries that formed soluble colorimetric reaction products within the void volume of patterned paper zones. ¹² However, unlike litmus paper or urine dipstick tests, colorimetric products in μPADs can have a non-uniform distribution within the test zone, which is caused either by unoptimized storage conditions (e.g., "coffee-ring effect" from dried reagents) or issues with balancing product diffusion or net fluid flow (i.e., by wicking). ^{24–26} Heterogeneous signals in test zones, regardless of whether devices are designed to be operated in two- or three-dimensional configurations, can result in interpretation errors, particularly when printed read guides are presented with colors that are uniform in hue and spatial position (**Figure S1**). ²⁷

A variety of strategies have been developed to address challenges related to the position and distribution of colorimetric signals in patterned paper zones. For assay formats that require molecular recognition, incorporation of nylon¹⁰ or nitrocellulose²⁸ membranes into device designs can support reagent immobilization by physisorption and capture of analytes under continuous flow. Alternatively, the surfaces of cellulosic paper fibers can be functionalized chemically^{29–31} or biochemically (e.g., via engineered proteins)^{32,33} to support the immobilization of reagents.^{34,35} Detection reagents can also be crosslinked throughout the open pore structure of a paper substrate to create an immobilized network of materials that would otherwise diffuse throughout the paper architecture.^{36,37} While these approaches provide assay developers with a variety of device design options, they each require target analytes to be captured or reagent-specific functionalization strategies to restrict the formation of a colorimetric signal to a defined location.

To generate spatially-controlled, colorimetric signals without the requirements for molecular recognition or reagent immobilization, we developed a new class of paper-based microfluidic devices that form and confine colorimetric signals to the interfaces of converging liquid fronts (**Figure 1A**). The fluidic network patterned into the device splits a single sample inlet into separate and ultimately opposing channels. Analytes can undergo partial reactions with unique reagents stored in each channel. The products of these partial reactions are directed towards a common test zone. Others have shown paper devices designed for the sequential, timed delivery of reagents from multiple channels that are directed towards a test zone. ^{38,39} In these devices, flow is continuous as long as sufficient volume is available to saturate the paper. Because paper-based devices are inherently self-metering, ⁵ if a single channel is split and recombined, net fluid flow stops when the advancing fluid fronts meet. At this interface between fronts, where reactions between previously separated reagents are now possible and controlled by diffusion, assay products can be isolated without affinity-based capture and lead to the formation of colorimetric signals that are confined to the contour of the interface. Using this device design strategy, we demonstrate the detection of multiple classes of analytes—ions, small molecules, and enzymes—

by producing line-format signals like those provided by LFTs but resulting from soluble reaction products. We demonstrate our approach by developing assays for iron (III), acetylcholinesterase, and lactate. Additionally, we demonstrate the scalability of this method by increasing the number of fluid fronts that converge in a common detection zone to create multiplexed assays: two converging channels create one interface (i.e., singleplex) while three or four converging channels create three or four interfaces, respectively (i.e., multiplex). We demonstrate the ability to create multiple lines in common zone by combining test and control assays for both iron (III) and acetylcholinesterase. Overall, these devices provide a new method of generating user-friendly signal formats for analytes that are currently incompatible with molecular recognition-style assay architectures.

Results and discussion

Device Design Considerations

The features patterned into the paper device autonomously control how a sample is split into opposing channels and recombined to form interfaces. The properties and quantities of reagents stored within paper layers determine rehydration times and the rates at which they wick through the device and toward the ultimate detection zone. For assays that require reagents with different chemical properties (e.g., solubility, rehydration rate, or interactions with the surrounding paper matrix) to be stored on opposite sides of the device, channel lengths may be adjusted to provide timed convergence of liquid fronts at the desired location. This approach is shown in **Figure S2A**, in which an interface formed between two solutions of colored dyes was shifted from the center of the device detection zone using an asymmetrical channel geometry. Additionally, the position of the formed interface is dependent on the geometries of patterned paper layer features and proper layer alignment (**Tables S1**, **Table S2**). We developed a layer alignment pin tool and protocol to position device features reproducibly and ensure the interface position is only dependent on synchronized delivery of fluid fronts to the detection zone (**Figure**

S3). This approach consistently provides interfaces at the center of device detection zones (**Figure S2B**). In the assays described below, a symmetrical channel design reproducibly afforded interfaces in the center of the test zone (**Figure S4**).

While evaluating the reproducibility of signal formation in these devices, we noticed that the background color intensity of the detection zones was influenced by the wax pattern from the preceding reagent storage layer now being visualized through the wet, semi-transparent paper zone. In other three-dimensional paper-based device designs, ¹⁰ output zones are typically backed by patterned paper channels, which are white in color to provide color contrast; zones are exposed in single-layer µPADs. In these interface-forming devices, however, detection zones are not in direct, vertical fluidic connection with patterned features on the previous layer. To enhance the contrast between colorimetric signal at liquid interfaces and the surrounding paper matrix, we altered our device design to include a patterned paper zone in the center of the reagent storage layer (**Figure S5**). A sheet of transparent laminate was added below the bottom layer to seal the device, prevent evaporation, and still visualize the result (**Figure S6**).

Analyte detection strategy

These paper devices perform assays through multistep or partial-step chemical reactions that are carried out in opposing channels but from a single sample input. The resulting colorimetric signal only forms when the advancing liquid fronts converge, and reagents and intermediate products can react by diffusing across the formed interface. In the single-analyte detection format, reagents are stored within the device such that one channel contains analyte-specific reagents, and the other channel contains a product-specific indicator. Upon introduction of the sample, a partial reaction occurs in the channel containing analyte-specific reagents. As the two liquid fronts converge, the assay is completed by reaction between the formed product and the product-specific indicator. Thus, a colorimetric interfacial signal develops in the readout zone and the

signal is confined in the interface contour due to reaction specificity and timed transport of solutions.

Quantifying interface signal

We performed signal analysis using ImageJ. 44 To analyze signal intensity at the interface, we either (i) used the "Plot Profile" tool and analyzed the pixel intensity across the circular signal readout region or (ii) defined the interfacial signal using the "Rectangle" tool and then performed "RGB Measure" analysis using the available plugin. The time required to generate visible signals can vary based on the grade of paper used to fabricate the device (Table S3). Additionally, we investigated the effect of applied sample volume on the absolute position, width, and color intensity of interfaces formed in our paper-based devices. We found that only volumes above 30 μL reach a plateau in the intensity of the interface signal, with no benefit observed using larger volumes. (Table S4). We used Whatman 4 for all layers of our paper-based device and observed that signal formation starts at approximately 2 minutes. Product generation accumulates over time and causes an increase in signal intensity, until saturating at approximately 7 minutes after the sample was added (Figure 2A). Additionally, the gradual increase in signal intensity causes nearly linear broadening of the width of the formed interface over time, which eventually compromises signal intensity. Therefore, we determined the ideal signal read time is between 7-10 minutes, with the cut off time for signal interpretation to be 20 minutes. Prior to the cut off time, the signal intensity is at a maximum value and can be used for qualitative detection, which we demonstrate with Fe(III) ions (Figure 2B). After the cut off time, the signal intensity diminishes over time due to diffusion of chromogenic products away from the interface.

Iron (Fe(III))

For the representative ion assay, we selected Fe(III). Iron homeostasis is vital to multiple biological processes (e.g., oxygen transport and short-term oxygen storage) and the

concentration of iron can be used as a diagnostic marker for anemia.⁴⁵ We chose Fe(III) as a model analyte to highlight two key functions of our device: (i) the separation of reduction and chelation reactions and (ii) the spatial confinement of low molecular weight products. To detect Fe(III), we stored ascorbic acid (a reducing agent) and 3-(2-pyridyl)-5,6-diphenyl-1,2,4-triazine-p,p'-disulfonic acid (Ferrozine; a colorimetric indicator of Fe(II))⁴⁶ in opposite channels of the reagent storage layer (**Figure 3A**). When a sample is added to the device, it is split uniformly into each channel where it rehydrates and can react with these stored reagents. If Fe(III) is present in the sample, it will be reduced to Fe(II) in the channel containing ascorbic acid, while no reactions will occur in the channel containing Ferrozine. When the two wicking fronts converge at the detection zone on the bottom layer of the device, reduced Fe(II) is chelated by Ferrozine and forms a purple signal at the formed interface (**Figure 3B**, **Figure S7**).

In some experiments, we observed a noticeable background signal in the channel containing Ferrozine that scaled with the concentration of added Fe(III) (**Figure S8**). The presence of this background color could negatively impact the performance of the Fe(III) assay (i.e., reduced specificity and increased limit of detection). This color could be caused by metal impurities in the paper itself or the potential for Fe(III) to be an interferent in the specific detection of Fe(II) by Ferrozine. We minimized the background signal by incorporating ethylenediaminetetraacetic acid (EDTA) in the Ferrozine side of the sample distribution layer. 49.50 We tested both the effect of different EDTA and Ferrozine concentrations on the signal to background ratio (**Tables S5 and S6**). As the concentration of Ferrozine increased, the intensities of both the signal formed at the readout zone and the background increased. The increase in background intensity did not negatively impact the signal to background ratio, which increased proportionally with the concentration of Ferrozine. However, the increase in signal to background ratio in the presence of EDTA was higher than that without using EDTA, which further suggests that the incorporation of EDTA provided superior results.

The addition of samples containing Fe(III) resulted in interfaces with colors whose intensities correlated linearly with concentration between 5.8–13.0 mM and had an LOD of 2.9 mM (Figure 3C). We chose this range of concentrations as it corresponds to the biologically relevant concentration of total iron that could be liberated from hemoglobin.⁵¹ While quantitative analysis is useful to characterize assay performance as changes are made to reagent conditions or device design, ultimately, we envision the application of this approach to be similar to how LFTs operate—using the formation (or absence) of a line as a qualitative indicator of the presence (or absence) of an analyte (Figure 3D).

Acetylcholinesterase (AChE)

For the representative enzyme assay, we selected AChE. AChE hydrolyzes the neurotransmitter acetylcholine into choline and acetic acid to terminate neurotransmission at the cholinergic synapse. Inhibition of AChE by organophosphates, heavy metals, or chemical warfare agents can block acetylcholine transmission and lead to organ failure and death. 52 We chose AChE as a model analyte to evaluate how interfaces were formed when reactions were governed by two time-dependent processes: (i) the activity of the enzyme (i.e., the analyte) and (ii) diffusion and mixing of reactants across the interface. To detect AChE, we stored acetylthiocholine chloride and 5,5'-dithiobis(2-nitrobenzoic acid) (DTNB, Ellman's reagent) on opposite sides of the reagent storage layer (Figure S9). When AChE is present in the added sample, it reacts with acetylthiocholine to produce acetic acid and thiocholine (Figure 4A). At the interface, the liberated sulfhydryl group on the thiocholine interacts with DTNB to generate 2-nitro-5-thiobenzoic acid and form a yellow signal that we could quantify with image analysis. As expected for an enzymatic assay, the signal intensities saturated over time. Similar to the Fe(III) assay, signal from AChE assay took approximately two minutes to start forming and increased in width and intensity over time. To ensure color saturation, we used the scans taken 10 minutes after sample addition to analyze the signal intensity formed at the interface. We performed nonlinear regression of the

data using a saturation growth model for concentrations of AChE ranging from 2–30 U/mL (**Figure 4B**). From the fit, we determined that there was a nearly linear relationship between the concentration of AChE and measured signal between 2–10 U/mL, and signals at higher concentrations were saturated and could be detected but not quantified. While the physiological range of AChE in plasma is greater than 8 U/mL,⁵³ exposure to dangerous chemical agents (e.g., organophosphates) results in a reduction of AChE activity into the linear range of this assay. While it can be hard to clearly detect yellow lines on white backgrounds with the naked eye, especially at lower analyte concentrations, this AChE assay remains useful to provide a visual reference for qualitative detection (i.e., "yes or no" presence of analyte). Given the versatility of our device design, it is possible to substitute assay reagents (i.e., other colorimetric substrates)⁵² for AChE to enhance signal contrast.

Lactate

For the representative small molecule assay, we selected lactate. Lactate is an intermediate in the metabolic anerobic carbohydrate pathway whose concentration in sweat changes with exercise. While exercising, undesired lactate accumulation in the active muscle can manifest as fatigue, soreness, and pain.⁵⁴ Also, sweat lactate can provide information about insufficient oxidative metabolism and pressure ischemia.⁵⁵ We chose lactate as a model analyte to demonstrate how the device can accommodate multistep reactions. To detect lactate, we stored (i) nicotinamide adenine dinucleotide (NAD+) and lactate dehydrogenase (LDH) and (ii) 3-(4,5-dimethylthiazol-2-yl)-2,5-diphenyltetrazolium bromide (MTT) on opposite sides of the second layer of the device (Figure 5A). Then on the third layer, we again stored NAD+/LDH below the first treated layer and phenazine methosulfate (PMS) below MTT (Figure S10). When a sample containing lactate is introduced and split by the sample distribution layer, the following reactions occur: (i) LDH converts lactate to pyruvate and (ii) transfers the liberated hydride ion to the costored NAD+ to produce NADH. In the other channel, both MTT and PMS are simply rehydrated.

When the split sample converges at the interface, PMS mediates an electron transfer from NADH to reduce MTT and produce a purple-colored formazan product.

For stable reagent storage and optimal performance, we tested different configurations of device layers, layer treatments, and drying conditions (i.e., light and temperature). From initial trials, we determined it is necessary to spatially separate PMS and MTT for reagent storage stability and to perform all manufacturing steps in the dark at room temperature. The addition of hydrazine buffer on the fourth layer of the device was to neutralize the co-produced pyruvate. For the lactate assay, the detected concentration range was 2–50 mM (Figure 5B). Unlike Fe(III) and AChE assays, we analyzed lactate assay results approximately 4 minutes after sample addition to avoid increased background signal over time. The high noise is likely due to both MTT and PMS reagents causing a yellow background color. Since the assay involves enzymatic reactions, we analyzed the results by nonlinear regression using a growth and saturation model. The data showed a nearly linear correlation between signal intensity (green channel) at concentrations of lactate less than 20 mM. At higher concentrations of lactate, the signal saturated and resulted in detectable but not quantifiable signal (Figure 5C). The nearly linear range of measurement is useful to quantify lactate in sweat, which decreases from 31 mM at the start of exercising to 12 mM at the point of exhaustion.

Multiplexed detection

In **Figure 1**, we demonstrated that it was possible to design a device such that multiple, independent channels (i.e., 3–4) could converge in a common zone to create multiple interfaces. While this preliminary experiment was performed with dyes stored in the device and rehydrated only with water, the results showed several useful features that were analogous to the singleplex format: (i) equal channel lengths and design symmetry could control the position of interfaces in a common zone, (ii) mixing only occurs across interfaces formed from advancing fronts, and (iii) net flow stops when the read zone is filled to allow reactions to be confined only to formed

interfaces. As a result, we evaluated the potential to create multiplexed assays using the interface device design by combining two of the aforementioned singleplex assays.

Taking inspiration from a standard LFT, which comprises a single test line and single control line, we aimed to demonstrate the ability of our devices to support multiple test and control lines in the same read zone. We chose to develop an assay for Fe(III) and AChE, which would produce four interfacial signals: one test line and one control line for each respective analyte.

Figure S11 depicts the conditions that introduce assay reagents into their required spatial locations (layer and channel). One major difference from the singleplex assays is that control interfaces require the storage and eventual introduction of the partial reaction products formed in the test interfaces—namely, ferrous iron (FeCl₂) and a free thiol (cysteine)—to react with stored indicators. After all four channels wick through to the final layer, the four resulting liquid fronts converge at the detection zone and form four interfacial signals. At the detection zone, a yellow interface formed at position 1 indicates the presence of AChE, a yellow interface formed at position 2 indicates the corresponding control line for AChE, a purple interface formed at position 3 indicates the presence of control line for Fe(III), and finally, a purple interface formed at position 4 indicates the presence of Fe(III). The resulting outputs for all possible combinations of analytes (positive and negative for each, with corresponding controls) are shown on Figure 6.

Conclusions

In this manuscript, we report a new class of paper-based microfluidic devices that uses converging liquid fronts to constrain the location where assay chemistries are performed within test zones. Like the ubiquitous lateral flow test, which serve as an inspiration for the readout format of these devices, the shape of the colorimetric assay product is a line. We made this design decision to facilitate how assay results are interpreted, ⁵⁷ either qualitatively or quantitively. Unlike lateral flow tests, however, these paper devices do not rely on molecular recognition or affinity capture to immobilize analytes of interest or colorimetric reagents. Instead, by converging and

halting two opposing wicking fronts, the location of soluble reaction products can be defined. While we show the potential for this device format to support colorimetric assays for Fe(III), acetylcholinesterase, and lactate, we believe that similar applications are possible for other analytes represented by these classes (i.e., ions, enzymes, and small molecules). Although the dynamic ranges of these acetylcholinesterase and lactate assays are physiologically relevant, the limit of detection of Fe(III)—appropriate for total iron bound to hemoglobin (ca. mM)—is higher than required to measure ferric iron in serum⁵⁸ or drinking water (ca. µM).⁵⁹ We expect that optimizing assay conditions, inclusive of choices of indicator and grade of paper, may enable assays for iron in these micromolar regimes. Nonetheless, the Fe(III) assay successfully demonstrates the potential of µPADs to localize products of colorimetric reactions with ions to line-format interfaces for ease of readout.

In addition to singleplex assays, we further demonstrate that multiplexed assays—where multiple fluid fronts carrying distinct reaction products and/or indicators—can be supported by this approach to form interfaces in paper test zones. Unlike in singleplex assays, where efforts to optimize assay conditions and formulate reagents for storage within the device have relatively limited variables, the creation of multiplexed assays requires deliberate attention to reagent compatibility and cross-reactivity to limit false positives and negatives. Even so, the opportunity to integrate positive controls, which are frequently missing from assays developed for paper-based microfluidic devices, would address a major requirement for point-of-care tests. Beyond their use as procedural controls, we anticipate that the intensities of these lines may have the potential to be used as visual comparators to estimate the concentration of the analyte in the sample. In total, the unique design of these devices has the potential to simplify the user experience and interpretation of critical results at the point-of-use, while broadening the analytical capabilities and ultimate utility of paper-based microfluidic sensors.

Acknowledgments

This material is based upon work supported by the National Science Foundation under Grant No. CBET-1846846. This work was additionally supported by Tufts University and a generous gift from James Kanagy.

References

- (1) Gasperino, D.; Baughman, T.; Hsieh, H. v.; Bell, D.; Weigl, B. H. *Ann. Rev. of Anal. Chem.* 2018, **11**, 219–244.
- Jauset-Rubio, M.; Svobodová, M.; Mairal, T.; McNeil, C.; Keegan, N.; Saeed, A.; Abbas, M. N.; El-Shahawi, M. S.; Bashammakh, A. S.; Alyoubi, A. O.; O'Sullivan, C. K. Sci. Rep. 2016, 6, 37732.
- (3) Urusov, A. E.; Zherdev, A. v.; Dzantiev, B. B. Biosensors 2019, 9, 89.
- (4) Posthuma-Trumpie, G. A.; Korf, J.; van Amerongen, A. *Anal. Bioanal. Chem.* 2009, **393**, 2, 569–582.
- (5) Berry, S. B.; Fernandes, S. C.; Rajaratnam, A.; DeChiara, N. S.; Mace, C. R. *Lab Chip* 2016, **16**, 3689–3694.
- (6) Murray, L. P.; Mace, C. R. Anal. Chem. 2022, **94**, 10443–10450.
- (7) Connelly, J. T.; Rolland, J. P.; Whitesides, G. M. *Anal. Chem.* 2015, **87**, 7595–7601.
- (8) Hsu, C. K.; Huang, H. Y.; Chen, W. R.; Nishie, W.; Ujiie, H.; Natsuga, K.; Fan, S. T.; Wang, H. K.; Lee, J. Y. Y.; Tsai, W. L.; Shimizu, H.; Cheng, C. M. *Anal. Chem.* 2014, **86**, 4605–4610.
- (9) Ge, L.; Wang, S.; Song, X.; Ge, S.; Yu, J. Lab Chip. 2012, **12**, 3150–3158.
- (10) Schonhorn, J. E.; Fernandes, S. C.; Rajaratnam, A.; Deraney, R. N.; Rolland, J. P.; Mace, C. R. *Lab Chip* 2014, **14**, 4653–4658.
- (11) Fernandes, S. C.; Walz, J. A.; Wilson, D. J.; Brooks, J. C.; Mace, C. R. *Anal. Chem.* 2017, **89**, 5654–5664.
- (12) Martinez, A. W.; Phillips, S. T.; Butte, M. J.; Whitesides, G. M.; Martinez, W.; Phillips, S. T.; Butte, M. J.; Whitesides, G. M. *Angew. Chem. Int. Ed.* 2007, **46**, 1318–1320.
- (13) Carrilho, E.; Phillips, S. T.; Vella, S. J.; Martinez, A. W.; Whitesides, G. M. Paper *Anal. Chem.* 2009, **81**, 5990–5998.
- (14) Dungchai, W.; Chailapakul, O.; Henry, C. S. Anal. Chem. 2009, **81**, 5821–5826.
- (15) Yu, J.; Ge, L.; Huang, J.; Wang, S.; Ge, S. Lab Chip 2011, **11**, 1286–1291.
- (16) Liu, H.; Crooks, R. M. J. Am. Chem. Soc. 2011, **133**, 17564–17566.
- (17) Wang, C. C.; Hennek, J. W.; Ainla, A.; Kumar, A. A.; Lan, W. J.; Im, J.; Smith, B. S.; Zhao, M.; Whitesides, G. M. *Anal. Chem.* 2016, **88**, 6326–6333.
- (18) Li, X.; Zwanenburg, P.; Liu, X. Lab Chip 2013, 13, 2609–2614.
- (19) Fu, E. Analyst 2014, **139**, 4750–4757.

- (20) Cate, D. M.; Dungchai, W.; Cunningham, J. C.; Volckens, J.; Henry, C. S. *Lab Chip* 2013, **13**, 12, 2397–2404.
- (21) Lewis, G. G.; Robbins, J. S.; Phillips, S. T. Anal. Chem. 2013, 85, 10432–10439.
- (22) Lewis, G. G.; Ditucci, M. J.; Phillips, S. T. Angew. Chem. Int. Ed. 2012, **51**, 12707–12710.
- (23) Yamada, K.; Suzuki, K.; Citterio, D. ACS Sens. 2017, 2, 8, 1247–1254.
- (24) Derda, R.; Tang, S. K. Y.; Laromaine, A.; Mosadegh, B.; Hong, E.; Mwangi, M.; Mammoto, A.; Ingber, D. E.; Whitesides, G. M. *PLoS One* 2011, **6**, e18940.
- (25) de Freitas, S. v.; de Souza, F. R.; Rodrigues Neto, J. C.; Vasconcelos, G. A.; Abdelnur, P. v.; Vaz, B. G.; Henry, C. S.; Coltro, W. K. T. *Anal. Chem.* 2018, **90**, 11949–11954.
- (26) Morbioli, G. G.; Mazzu-Nascimento, T.; Stockton, A. M.; Carrilho, E. *Anal. Chim. Acta.* 2017, **970**, 1–22.
- (27) Pollock, N. R.; Rolland, J. P.; Kumar, S.; Beattie, P. D.; Jain, S.; Noubary, F.; Wong, V. L.; Pohlmann, R. A.; Ryan, U. S.; Whitesides, G. M. *Sci. Transl. Med.* 2012, **4**, 152.
- (28) Liu, M.; Hui, C. Y.; Zhang, Q.; Gu, J.; Kannan, B.; Jahanshahi-Anbuhi, S.; M Filipe, C. D.; ohn Brennan, J. D.; Li, Y.; *Angew. Chem. Int. Ed.* 2016, **55**, 2709–2713.
- (29) Kwong, P.; Gupta, M. *Anal. Chem.* 2012, **84**, 10129–10135.
- (30) Cheng, C.; Gupta, M. *Ind. Eng. Chem. Res.* 2018, **57**, 11675–11680.
- (31) Devadhasan, J. P.; Kim, J. Sens. Actuators. B Chem. 2018, 273, 18–24.
- (32) Miller, E. A.; Baniya, S.; Osorio, D.; al Maalouf, Y. J.; Sikes, H.D. *Biosens. Bioelectron.* 2018, **102**, 456–463.
- (33) Cavazos-Elizondo, D.; Sung, K-J.; Vasikaran, S.; Aguirre-Soto, A.; Sikes, H.D. *ACS Appl. Bio Mater.* 2021, **4**, 392–398.
- (34) Xiao, W.; Huang, J. *Langmuir* 2011, **27**, 12284–12288.
- (35) Nery, E. W.; Kubota, L. T. J. Pharm. Biomed. Anal. 2016, 117, 551–559.
- (36) Riccardi, C. M.; Mistri, D.; Hart, O.; Anuganti, M.; Lin, Y.; Kasi, R. M.; Kumar, C. V.; *Chem. Commun.* 2016, **52**, 2593–2596.
- (37) Wilson, D. J.; Martín-Martínez, F. J.; Deravi, L. F. ACS Sens. 2022, **7**, 523–533.
- (38) Strong, E. B.; Knutsen, C.; Wells, J. T.; Jangid, A. R.; Mitchell, M. L.; Martinez, N. W.; Martinez, A. W. *Inventions* 2019, **4**, 20.
- (39) Fu, E.; Lutz, B.; Kauffman, P.; Yager, P. Lab Chip 2010, **10**, 918–920.

- (40) Fridley, G. E.; Le, H. Q.; Fu, E.; Yager, P. Lab Chip 2012, 12, 4321–4327.
- (41) Noviana, E.; Ozer, T.; Carrell, C. S.; Link, J. S.; McMahon, C.; Jang, I.; Henry, C. S. *Chem. Rev.* 2021, **121**, 11835–11885.
- (42) Morbioli, G. G.; Mazzu-Nascimento, T.; Milan, L. A.; Stockton, A. M.; Carrilho, E. *Anal. Chem.* 2017, **89**, 4786–4792.
- (43) Lewis, G. G.; Ditucci, M. J.; Baker, M. S.; Phillips, S. T. Lab Chip 2012, **12**, 2630–2633.
- (44) Schneider, C.A.; Rasband, W.S.; Eliceiri, K.W. *Nat. Methods* 2012, **9**, 671–675.
- (45) Winter, W. E.; Bazydlo, L. A. L.; Harris, N. S. Lab. Med. 2014, 45, 92–102.
- (46) Stookey, L. L. Anal. Chem. 1970, 42, 779–781.
- (47) Lucchesi, C. A.; Hirn, C. F. Anal. Chem. 1960, 32, 1191–1193.
- (48) Im, J.; Lee, J.; Löffler, F. E. *J. Microbiol. Methods* 2013, **95**, 366–367.
- (49) Nguyen, T. H.; Waterhouse, A. L. J. Agric. Food Chem. 2019, 67, 680–687.
- (50) da Silva Santos, É.; de Melo Teixeira, L.; Castro, J. C.; Mardigan, L. P.; dos Santos, J. R.; Gonçalves, J. E.; de Oliveira, A. J. B.; Gonçalves, R. A. C. *Acta. Sci. Biol. Sci.* 2022, **44**, 1.
- (51) Johnson-Wimbley, T. D.; Graham, D. Y. *Therap. Adv. Gastroenterol.* 2011, 4, 177–184.
- (52) Liu, D. M.; Xu, B.; Dong, C. Trends Anal. Chem. 2021, **142**, 116320.
- (53) Panraksa, Y.; Siangproh, W.; Khampieng, T.; Chailapakul, O.; Apilux, A. *Talanta* 2018, **178**, 1017–1023.
- (54) Xuan, X.; Pérez-Ràfols, C.; Chen, C.; Cuartero, M.; Crespo, G. A. ACS Sens. 2021, **6**, 2763–2771.
- (55) Derbyshire, P. J.; Barr, H.; Davis, F.; Higson, S. P. J. *J. Physiol. Sci.* 2012, **62**, 429–440.
- (56) Koike, K.; Urata, Y.; Hiraoka, N. J. Clin. Biochem. Nutr. 1990, **9**, 151–161.
- (57) Murray, L. P.; Mace, C. R. Anal. Chim. Acta. 2020, **1140**, 236–249.
- (58) Mazzaracchio, V.; Bagheri, N.; Chiara, F.; Fiore, L.; Moscone, D.; Roggero, S.; Arduini, F. *Anal. Bioanal. Chem.* 2023, **415**, 1149–1157.
- (59) United States Environmental Protection Agency (US EPA), https://www.epa.gov/sdwa/drinking-water-regulations-and-contaminants, (Accessed June 2023).

Figure 1. Schematics of three-dimensional paper-based devices designed to form single and multiple liquid interfaces in a single detection zone. (A) Unique device geometries can be designed to form one-line, three-line, and four-line interface patterns. Dashed lines indicate fluid flow within and between layers. Upon application of a sample, fluid is distributed to opposite sides of the device to rehydrate stored reagents. After rehydration, solutions are directed toward a central detection zone where they meet to form a liquid interface. (B) In these examples, colored dyes were used to demonstrate interfacial signal development. The detection zone is approximately 5 mm in diameter.

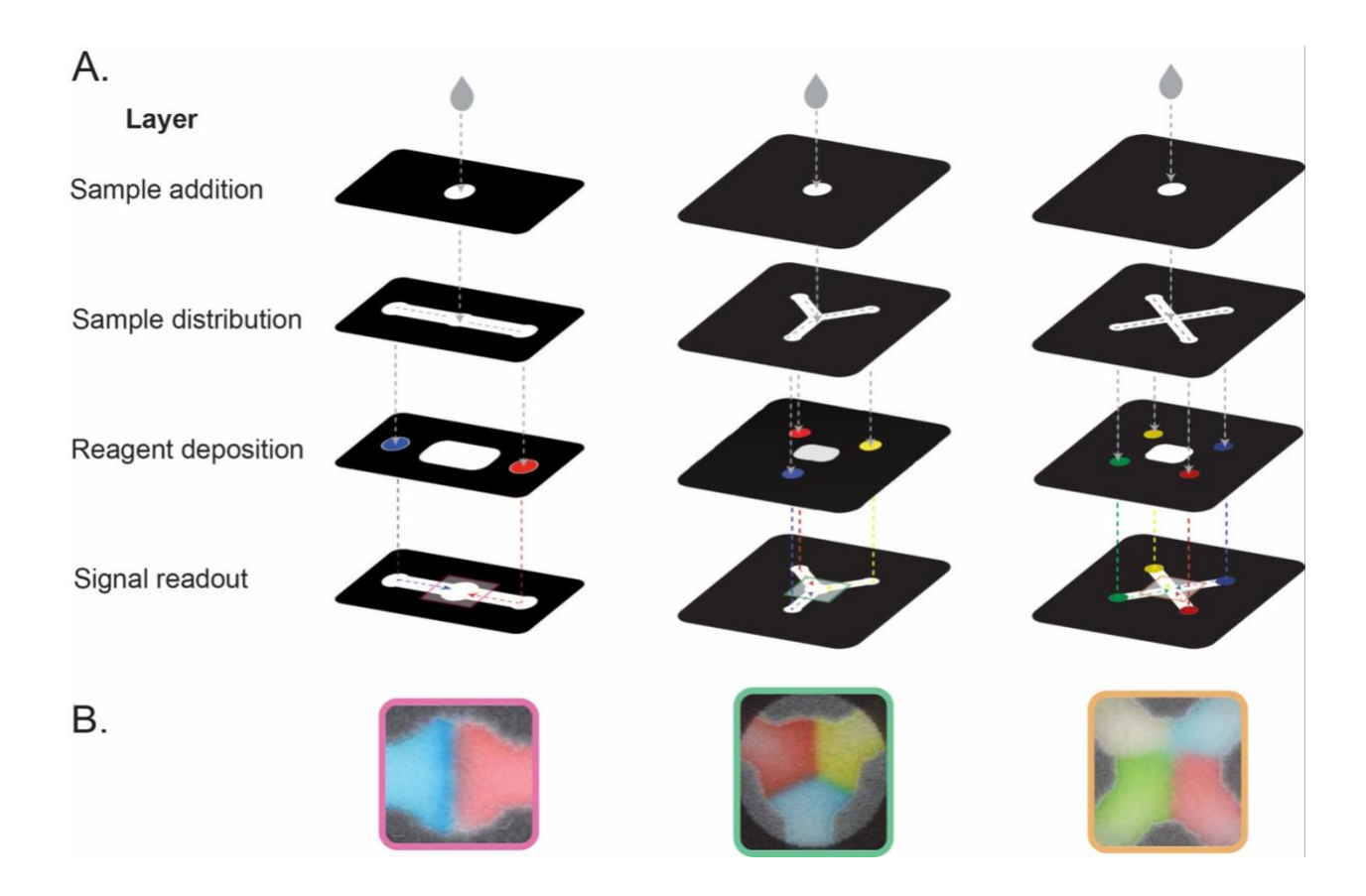


Figure 2. Results of experiments to evaluate the effect of reaction time on the intensity (A) and width (B) of assay interfaces for the colorimetric detection of Fe(III). When opposing wicking fronts converge in the test zone, assay reagents (a reduced Fe(II) products and Ferrozine, a specific indicator for Fe(II)) can react by diffusing across the interface formed when flow stops. We used (A) a saturation growth model to fit the relationship between the signal intensity (quantified via red channel for the purple reaction product) and time, and (B) linear regression to fit the relationship between the width of the colored interface and time. Error bars represent standard error of the mean for n = 5 measurements. Detection zones are approximately 5 mm in diameter.

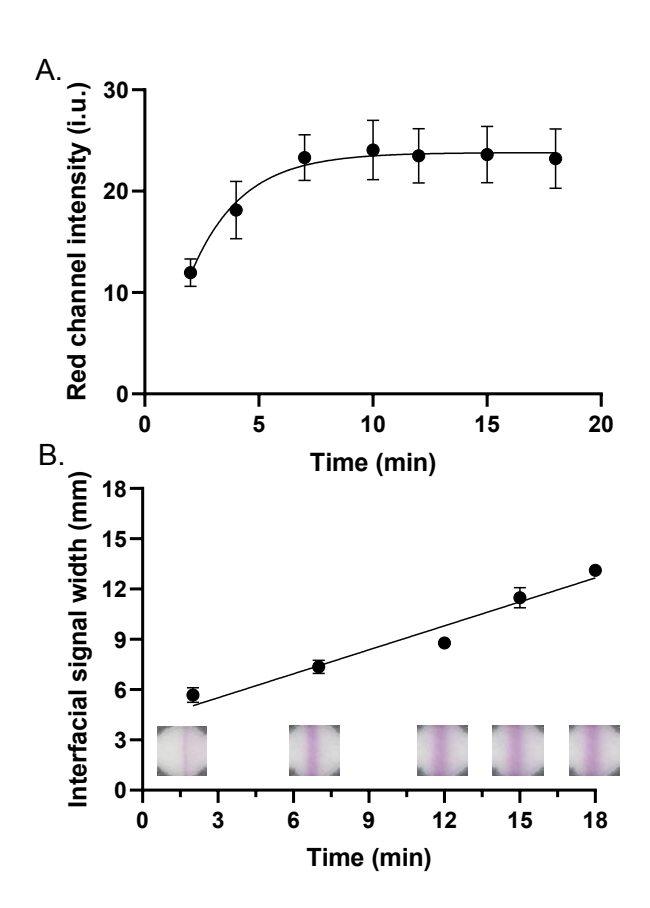


Figure 3. Fe(III) assay design strategy. (A) Schematic of fluid flow in the multilayer device. The sample is distributed to separate channels containing partial reagents responsible for the complete reaction. On one side of the device, Fe(III) is reduced to Fe(II) by ascorbic acid. On the other side of the device, the Ferrozine colorimetric indicator for the reaction product is rehydrated and transported to the detection zone. (B) When solution fronts converge in the detection layer, diffusion across a formed liquid interface facilitates the formation of colorimetric signals. (C) Resulting calibration curve for quantitative detection of Fe(III). Error bars represent standard error of the mean for n = 5 measurements. (D) Scans of detection zone with interfaces formed at different concentrations. Detection zones are approximately 5 mm in diameter.

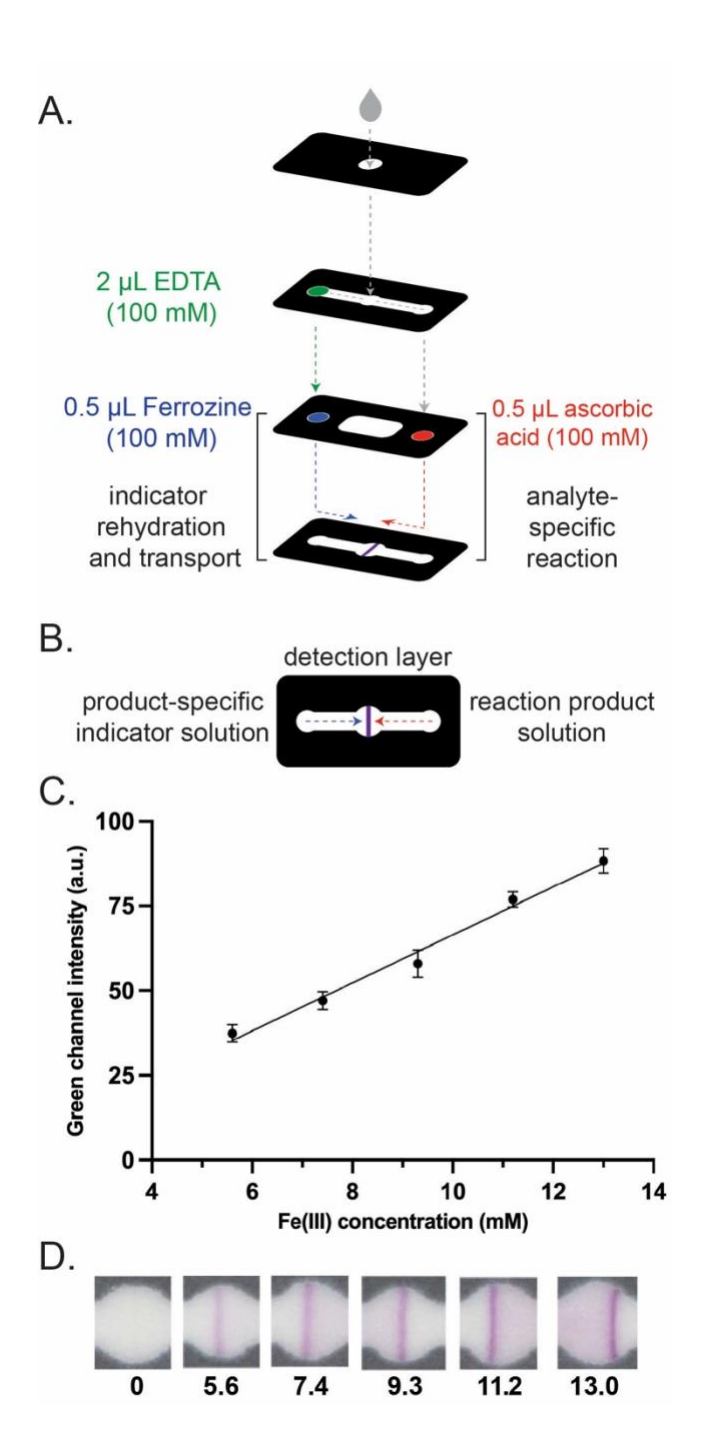


Figure 4. Acetylcholinesterase (AChE) assay design strategy. (A) Simplified schematic for the assay chemistry that focuses on the reactions that occur in each layer and arm of the three-dimensional paper-based device, which leads to the specific formation of color (yellow) at the interface formed between combined fluid fronts. (B) Resulting calibration curve for quantitative detection of AChE. A saturation growth model was applied for non-linear regression of the measured signal as a function of AChE concentration. Error bars represent standard error of the mean for n = 5 measurements. (C) Scans of detection zones with interfaces formed at different concentrations. Detection zones are approximately 5 mm in diameter.

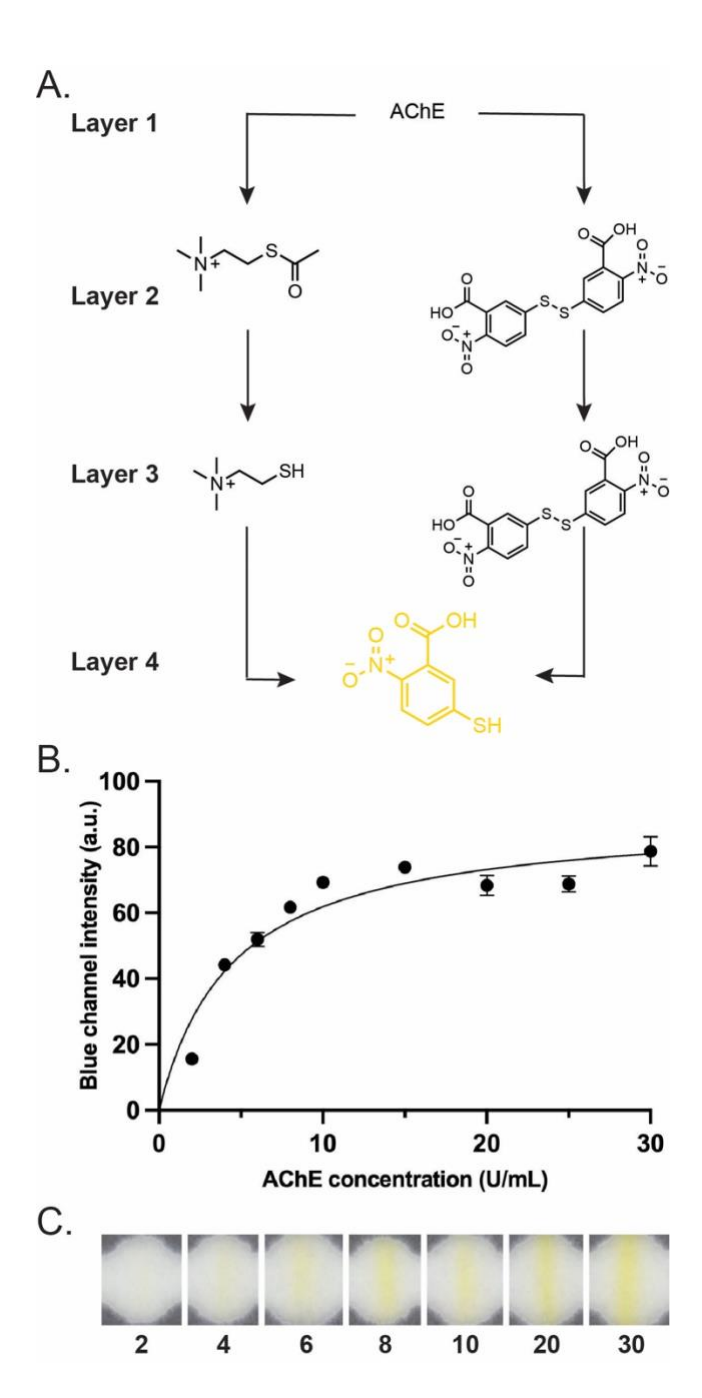


Figure 5. Lactate assay design strategy. (A) Simplified schematic for the assay chemistry that focuses on the reactions that occur in each layer and arm of the three-dimensional paper-based device, which leads to the specific formation of color (blue/purple) at the interface formed between combined fluid fronts. (B) Resulting calibration curve for quantitative detection of lactate. A saturation growth model was applied for non-linear regression of the measured signal as a function of lactate concentration. Error bars represent standard error of the mean for n = 5 measurements. (C) Scans of detection zone with interfaces formed at different concentrations. Detection zones are approximately 5 mm in diameter.

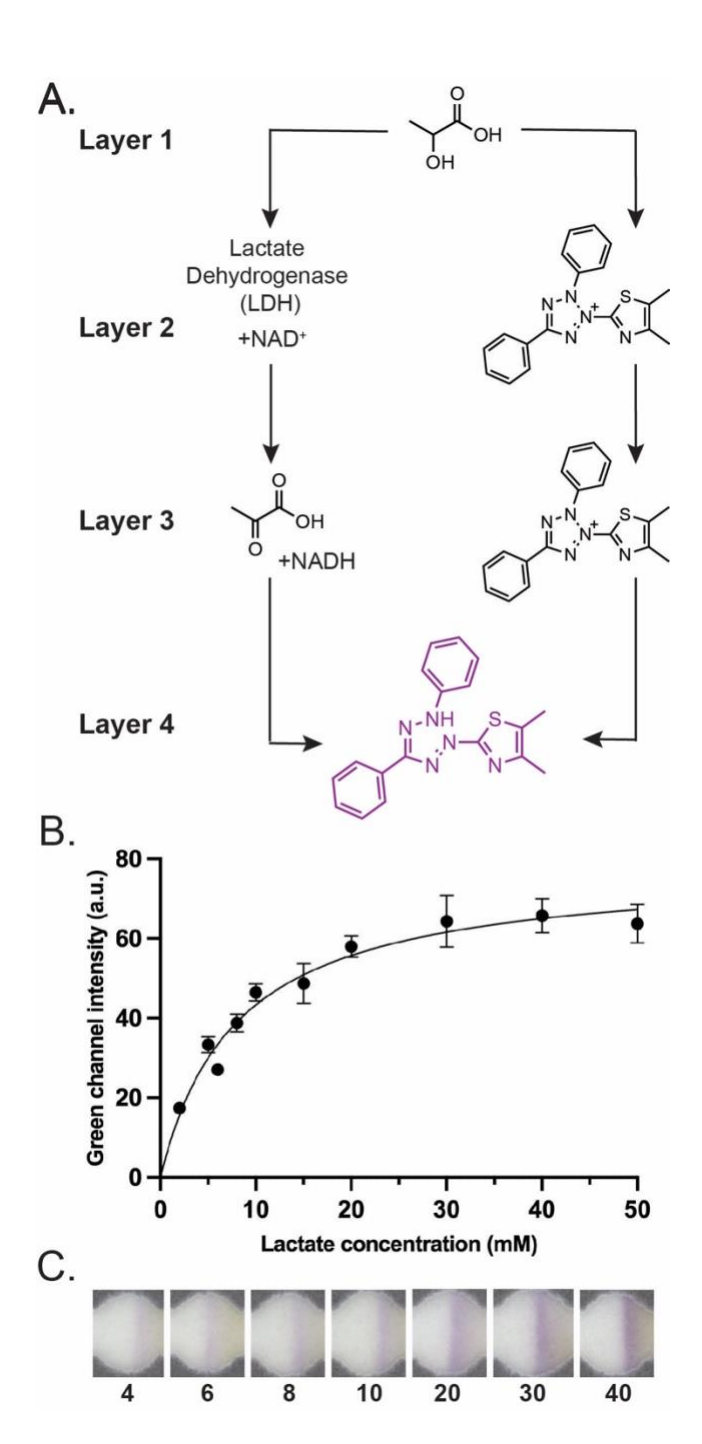


Figure 6. Demonstration of multiplexed assays in a common detection zone due to the convergence of multiple fluid fronts. Scans of detection zones showing interface patterns formed from combinations of tests and positive controls for Fe(III) and acetylcholinesterase (AChE) assays. Lines can be formed along all four coordinate positions according to the analyte and/or control they represent. The far left circle depicts a map of where signals will be formed for tests and controls of Fe(III) and AChE assays. Images of detection zones are accompanied by an individual map of the lines expected to be formed by a given experiment. Detection zones are approximately 5 mm in diameter.

